Vesicle-bound regulatory RNAs are associated with tissue aging

Fabian Kern[1,#], Thomas Kuhn[2,3,#], Nicole Ludwig[4,5,#], Martin Simon[6,#], Laura Gröger[4], Natalie Fabis[6], Abdulrahman Salhab[7], Tobias Fehlmann[1], Oliver Hahn[8], Annika Engel[9], Marcus Koch[10], Jana Koehler[9], Katarzyna Winek[11], Hermona Soreq[11], Gregor Fuhrmann[2,3], Tony Wyss-Coray[8], Eckart Meese[4], Matthias W. Laschke[12,&], Andreas Keller[1,8,13,&,*]

1 Chair for Clinical Bioinformatics, Saarland Informatics Campus, Saarland University, 66123 Saarbrücken, Germany
2 Helmholtz-Institute for Pharmaceutical Research Saarland (HIPS), Helmholtz-Centre for Infection Research (HZI), Biogenic Nanotherapeutics group (BION), 66123 Saarbrücken, Germany
3 Department of Pharmacy, Saarland University, 66123 Saarbrücken, Germany
4 Department of Human Genetics, Saarland University, 66421 Homburg, Germany
5 Center for Human and Molecular Biology, Saarland University, 66421 Homburg, Germany
6 Department of Biochemistry, Wuppertal University, 42119 Wuppertal, Germany
7 Department of Genetics and Epigenetics, Saarland University, 66123 Saarbrücken, Germany
8 Department of Neurology and Neurological Sciences, Stanford University, Stanford, 94304 CA, USA
9 German Research Center for Artificial Intelligence, 66123 Saarbrücken, Germany
10 INM – Leibniz Institute for New Materials, Campus D2 2, 66123 Saarbrücken, Germany
11 The Edmond and Lily Safra Center for Brain Sciences, The Hebrew University of Jerusalem, Jerusalem, Israel
12 Institute for Clinical and Experimental Surgery, Saarland University, 66421 Homburg, Germany
13 Center for Bioinformatics, Saarland University, 66123 Saarbrücken, Germany

# These authors have equally contributed to the study and are listed in lexicographic order
& These authors contributed equally as senior authors to the study
* Correspondence should be addressed to Andreas Keller (andreas.keller@ccb.uni-saarland.de, +49 174 1684638)

1 Previous work on murine models and human demonstrated global as well as tissue-specific
2 molecular aging trajectories in solid tissues and body fluids[1-8]. Extracellular vesicles like
3 exosomes play a crucial role in communication and information exchange in between such
4 systemic factors and solid tissues[9,10]. We sequenced freely circulating and vesicle-bound small
5 regulatory RNAs in mice at five time points across the average life span from 2 to 18 months.
6 Intriguingly, each small RNA class exhibits unique aging patterns, which showed differential
7 signatures between vesicle-bound and freely circulating molecules. In particular, tRNA
8 fragments showed overall highest correlation with aging which also matched well between
9 sample types, facilitating age prediction with non-negative matrix factorization (86% accuracy).
10 Interestingly, rRNAs exhibited inverse correlation trajectories between vesicles and plasma
11 while vesicle-bound microRNAs (miRNAs) were exceptionally strong associated with aging.
12 Affected miRNAs regulate the inflammatory response and transcriptional processes, and
13 adipose tissues show considerable effects in associated gene regulatory modules. Finally,
14 nanoparticle tracking and electron microscopy suggest a shift from overall many small to fewer
15 but larger vesicles in aged plasma, potentially contributing to systemic aging trajectories and
16 affecting the molecular aging of organs.
17
18 **Keywords:** non-coding RNA; tissue aging; extracellular vesicles; plasma; exosomes

Introduction

Understanding and controlling molecular hallmarks of age- related processes in higher organisms promises to greatly improve the quality of life[1]. For humans, aging is frequently studied using easily accessible biospecimens such as blood, serum or urine. Consequently, the scientific community generated models for a broad spectrum of molecular physiological and pathophysiological processes from different molecule types. For example, studies rely on long-lived individuals[2], serum proteomic profiling[3], small RNA patterns in blood cells[4,11], or the exploration of epigenetic control of aging clocks[5]. Likewise, deeper profiles such as gene expression fingerprints are available for different tissues[6]. Murine models facilitate the analysis of such processes thanks to their restricted influence of a heterogenous genetic background and varying lifestyles as compared to humans. Thus, organism-wide RNA-sequencing data of major organs and cell types across the mouse lifespan are available as unique resource to study aging[7,8]. The available data suggest complex aging patterns, including both linear and non-linear effects that are either specific for organs or follow more global organism-wide trajectories. These observations indicate a systemic and well-orchestrated exchange of information and molecules between organs. Specifically, extracellular vesicles (EVs) such as exosomes are postulated to play an important role[9,10], e.g., hypothalamic stem cells seem to control aging through exosomal miRNAs[12]. Recently, targeted intervention of exosomal transfer of miRNAs from osteoclast to chondrocytes was described as promising method to slow or even inhibit osteoarthritis in mice[13], as also summarized in a news and views article [14]. Further, several studies address the relation of EVs with aging in a systematic manner[15-18]. Also of special interest are studies investigating the change of vesicle bound non-coding RNAs depending on (treatment) interventions such as caloric restriction[19]. However, these studies are often limited in their analysis scope by considering only one small RNA class at a time and even restricting themselves to a subset of well characterized representatives. Moreover, an inherent restriction often is the limited sample count, frequently leading to pooling of biosamples and blurring fine-grained signals.

These and other issues complicate the analysis of EVs and their molecular load. Especially in the context of EVs in cancer, common pitfalls in purification have been summarized by Schekman and co-workers[20] with the correct nomenclature of EVs, purification and other aspects elucidated in great detail. Similar limitations as described in the context of cancer in this review also apply for other diseases, matrices and organisms.

For advancing our understanding on how systemic non-coding RNAs are associated with aging, we sought to discern differences between the molecular information included in EV cargo and freely circulating non-coding RNAs. We thereby balance the tradeoff of having sufficient material for high-throughput sequencing of individual plasma samples at the highest

55　purity of input material. For each
56　individual mouse, plasma and EV
57　samples we sequenced non-coding
58　RNAs and contrasted them by
59　computational approaches.
60
61　**Results**
62　　　　To uncover age-related
63　dynamic processes and to model the
64　information exchange involved we
65　sequenced both free circulating non-
66　coding RNAs and vesicle-bound
67　non-coding RNAs from individual
68　mice. The molecular profiles are
69　available at five time points across
70　the average lifespan between two to
71　18 months in two to four replicates
72　per age group and biospecimen type
73　(***Fig. 1A, Supplemental Table 1***).
74　For the plasma and the EV RNA
75　samples, we sequenced on average
76　38 million reads and mapped them
77　to ten different non-coding RNA
78　classes. In total, the feature set
79　includes 80,688 different non-coding
80　RNAs in mice, mostly piRNAs,
81　circRNAs, lincRNAs and miRNAs
82　(***Fig. 1B***). The very first aspect
83　encompassed the distribution of
84　molecules from the different RNA
85　classes. While tRNA fragments were
86　highly　represented　both　in
87　exosomes and as freely circulating
88　molecules, piRNAs showed sharply

89　lower levels in both specimen types (***Fig. 1C***). However, dominantly for circRNAs and rRNAs
90　significantly different amounts as freely circulating molecules compared to vesicle-bound
91　RNAs were observed. Notably, this analysis has a quantitative and RNA class centric view but
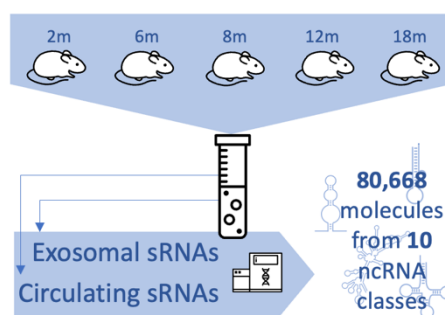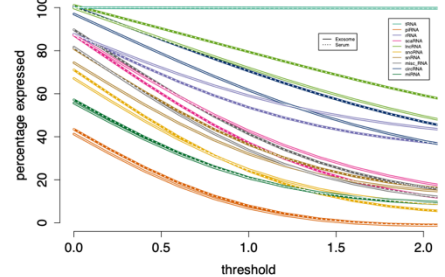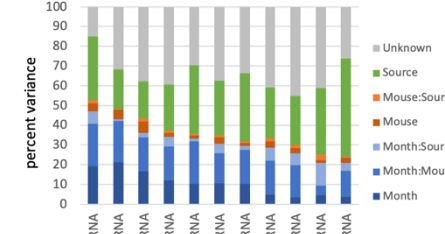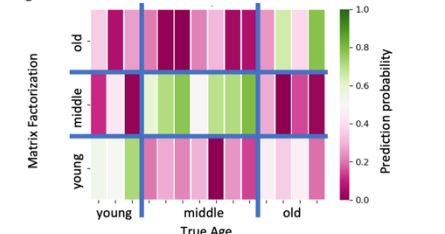
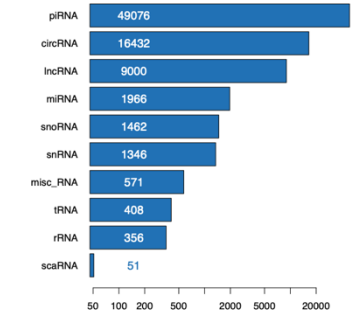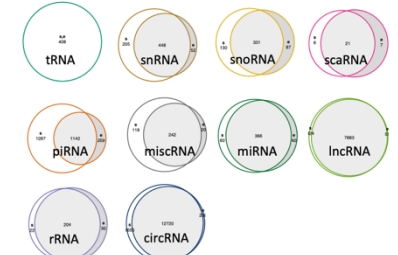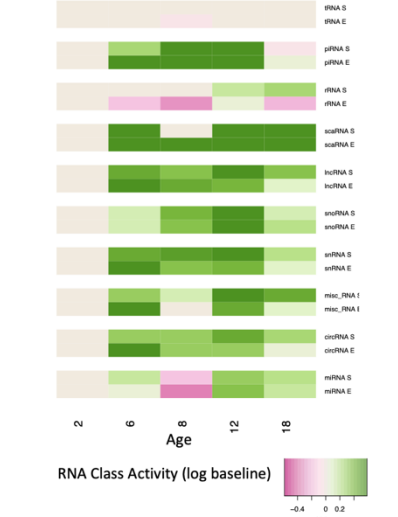**Figure 1**: Distribution of sequencing reads into their mapped non-coding RNA classes and their general relation to aging. (**A**) Study set-up. We profiled vesicle and plasma samples from mice in 5 age groups and sequenced 80,668 non-coding RNAs from 10 classes. (**B**) Overall distribution of molecules to the 10 non-coding RNA classes. (**C**) Fraction of representatives per RNA class dependent on an expression threshold. Dashed lines are serum, solid lines vesicle samples. (**D**) Overlap of expressed RNAs in plasma and vesicles as area proportional Venn diagrams. (**E**) percent of total data variance attributed to different parameters such as the age (month), individual mice or specimen type (source). Columns are sorted according to decreasing fraction of variance attributed to the age. (**F**) Relative expression of the different RNA classes per timepoint and sample type as compared to the baseline (2 months). Green means higher expression and purple lower expression. The upper row per RNA class is serum, the lower row is vesicles. (**G**) Prediction of age by non-negative matrix factorization. The color code represents the probability (trust) in the prediction, x-axis represents the true age group, y-axis the predictions.

92   does not yet consider whether the representative within the classes match across sample

93   types. For example, only a small number of piRNAs are expressed both in plasma and

94   exosomes even though general abundance was high. Considering the sample type overlap for

95   each class, indeed the most significant difference was observed between circulating and

96   vesicle-bound piRNAs (*Fig. 1D*). Similarly, we report large differences in the content of RNA

97   molecules from snRNAs, snoRNAs, and scaRNAs. In contrast, detected tRNA fragments,

98   lincRNAs, rRNAs and circRNAs are often shared between the two specimen types. In sum,

99   our data thus argue for a type-specific expression patterns that differ significantly between

100 non-coding RNA classes in a quantitative and qualitative manner.

101   Our initial hypothesis was to test for unique aging trajectories within and between non-

102 coding RNA classes wrapped in vesicles or freely circulating in plasma. Thus, we computed

103 the proportions of variance in the RNA counts that can be explained by available sample

104 metadata, i.e., either by age of the mice, the specimen type and donor mice identity, or linear

105 combinations of such. Here, tRNA fragments and miRNAs clearly stood out in terms of fraction

106 of variance explained by the age (*Fig. 1E*). In comparison, the lowest information content with

107 respect to age was obtained by scaRNAs and rRNAs. Importantly, the individuality factor of

108 each donor mice used for this study was comparably small, independent of the RNA class. To

109 uncover the actual relationship between each RNA class and mice age, we set the expression

110 at month 2 as baseline and modelled whether activity increases or decreases over time in EVs

111 and plasma, separately. As one result, we found remarkably similar dynamics of change for

112 vesicles and free circulating RNAs.

113   The largest overall age-related differences exist in rRNAs where the overall amount

114 increases for free circulating molecules with aging but the vesicle loading of rRNAs decreases.

115 This substantial difference in the specimen types also explains the high proportion of variance

116 attributed to the sample type annotation (rightmost green bar in *Fig. 1E*). Our data further

117 indicate a strong aging signal in EVs and in plasma, with varying strengths, again depending

118 on the RNA class (*Fig. 1F*). As our previous analyses emphasized the role of tRNA fragments,

119 we investigated the expression profiles in an unbiased manner and performed a classification

120 into three age groups (young, 2 months; middle aged, 6-8 months; old, 12-18 months). We

121 modelled this classification task as optimization problem through non-negative matrix

122 factorization, computing probabilities for each sample to belong to each of the three age

123 groups. We then assigned each sample to the age group with highest probability. For both

124 plasma and micro-vesicles, we got varying prediction accuracies, once again with the best

125 results for tRNA fragments with a remarkable accuracy of 86% (*Fig. 1G*).

126   Taken together, our analyses suggest non-coding RNAs to exhibit specific age

127 trajectories, both in qualitative and quantitative aspects. Moreover, the data pinpoint at

128 substantial differences in case of circulating RNAs and vesicle bound RNAs where the best

129   correlation with age was observed for tRNA fragments. This immediately poses the question
130   whether loading of vesicles follows biologically relevant environmental mechanisms. To
131   discover such potential patterns, we next performed a fine-granular and molecule-centric
132   analysis.

133   From the 80,668 unique non-coding RNA molecules in *Mus musculus* included in our
134   analysis, 23,052 (28.6%) are stably expressed in plasma and vesicles (**Supplemental Table
135   2**). We then computed the linear Pearson correlation as well as the non-linear distance
136   correlation for each of the investigated RNAs.

137   Based on this information, we estimated for each RNA whether it is linearly correlated
138   with age, nonlinearly correlated with age or not correlated with age at all for plasma and
139   vesicles separately. For both sample types, freely circulating in plasma (**Fig. 2A**) and vesicle
140   bound (**Fig. 2B**), the linear component was dominant and online few exceptions with non-linear
141   trajectories occurred. The amplitude and frequency of non-linear RNAs were both slightly
142   enriched in EVs. Interestingly, we also observed a slight enrichment towards negative
143   correlation in EVs. Both aspects argue for a more characteristic abundance of RNA levels in
144   aging EVs as compared serum. Having observed non-coding RNAs that are positively and
145   negatively correlated with age in vesicles or freely circulating further called for exploring
146   whether the up- and down-regulated molecules show similar compositions in the two specimen
147   types. In total, 27% and 22% are increasing and decreasing with age in EVs and serum,
148   respectively, slightly differing from what would be expected by a random distribution (cf.
149   methods). Intriguingly, however 39% of the 23,052 expressed non-coding RNAs are negatively
150   correlated in EVs with age but positively correlated in plasma and with 12% behaving vice-
151   versa (**Fig. 2C, Supplemental Table 2**). To seek common patterns for the increasing and
152   decreasing expression of non-coding RNAs we clustered the expression in EVs and in plasma
153   separately and extracted RNA clusters from the dendrogram. For each cluster we then
154   computed the average linear and non-linear correlation with aging and finally calculated the
155   overlap of the sample types. Our analysis confirmed the strong and orchestrated decrease of
156   correlation with age in EVs as compared to plasma **(Fig. 2D)**. The vesicle clusters are enriched
157   in the lower left corner, indicating the significant trend towards negative correlation with age in
158   EVs. Further, the data reveals a substantial age-related loss in linear correlation as compared
159   to non-linear correlation. To validate the origin of these signals we inspected all concordant
160   and discordant non-coding RNAs and provide specific examples for markers clearly increasing
161   with age in plasma and vesicles *(miR-466i-5p, **Fig. 2E**)*, decreasing with age in plasma and
162   vesicles *(Gm16701, **Fig. 2F**)*, increasing with age in plasma but decreasing with age in vesicles
163   *(Gm20756, **Fig. 2G**)*, and lastly decreasing with age in plasma but increasing in vesicles *(miR-
164   690, **Fig. 2H**)*. We further examined whether the patterns hold for all the 10 non-coding RNA

classes or rather if they are class specific. Here, the specificity of patterns for the different non-coding RNA classes was astonishing. For example, 94% of tRNA fragments increased with age in both plasma and in EVs. Also, 54% of rRNAs decreased with age in plasma but increased with age if vesicle-bound. Inversely, 42% of circRNAs increased with age in plasma but increased with age if vesicle-bound. Also, other RNA classes revealed distribution patterns significantly deviating from the 25% per group as expected by chance. For example, 82% of miRNAs increased with age in EVs *(Fig. 2I)*.

In the light of the regulatory mechanism of miRNAs typically repressing gene expression[21] and further knowing that mRNA levels tend to decrease with age, we next asked
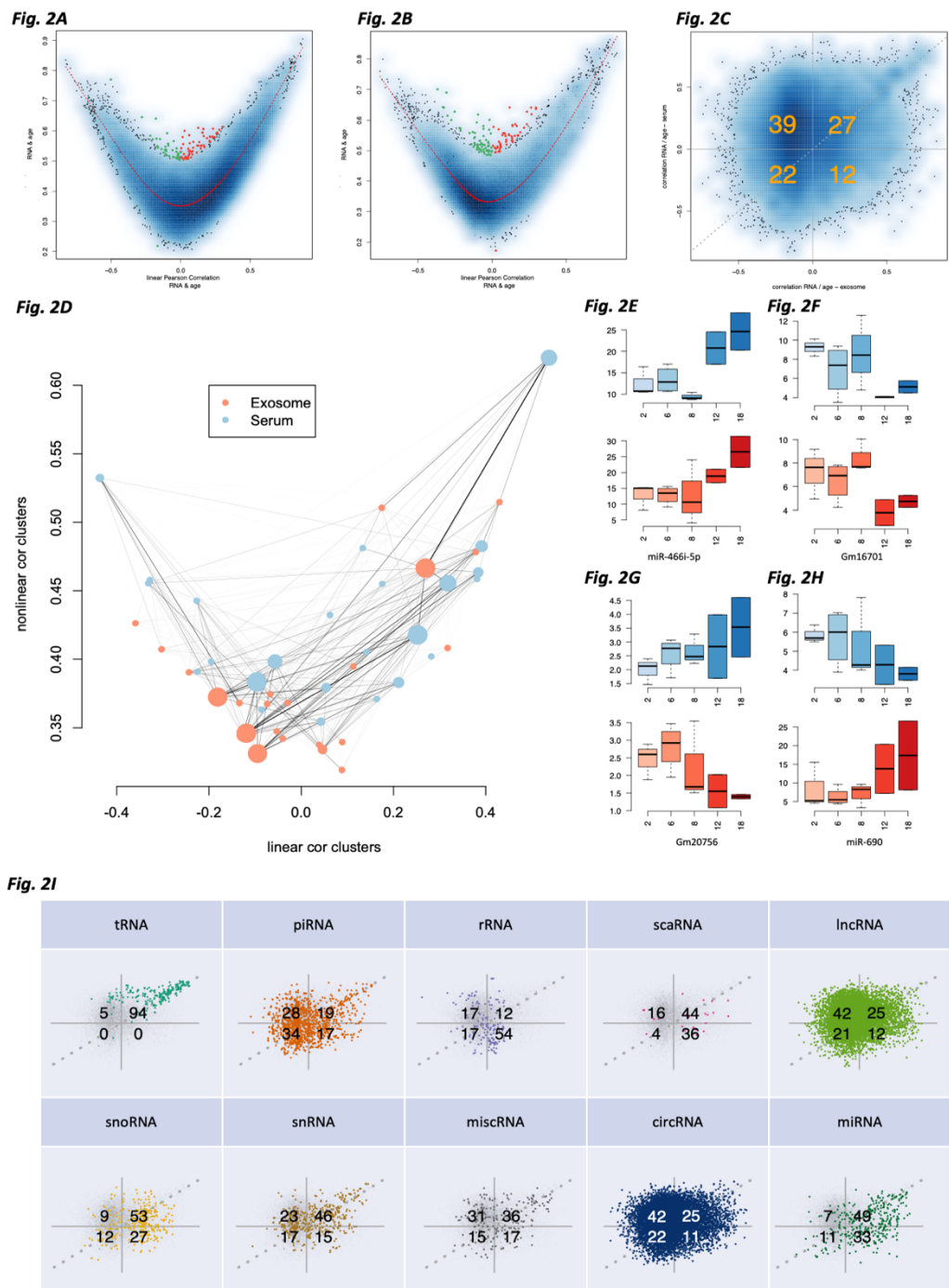

Figure 2: Correlation of non-coding RNAs with aging in EVs and in serum. (**A**) For each non-coding RNA, the x-axis represents the Pearson correlation and the y-axis the distance correlation with age in serum. The red line is a smoothed spline, and the colored dots (green, negatively; red, positively) are correlated with age in a predominantly non-linear manner. (**B**) The same information as in panel (A) but for EVs. (**C**) Scatter plot showing the Pearson correlation in vesicles (x-axis) in relation to the Pearson correlation in plasma (y-axis). Orange numbers represent the percentage of points in each of the four quarters. The data suggest a shift to negative correlation with age in vesicles. (**D**) Non-coding RNAs in plasma and EVs were clustered and resulting clusters were attributed with the average linear and non-linear correlation. Solid lines represent a match of non-coding RNAs, the thicker the line the more non-coding RNAs match between a plasma and vesicle cluster. The diameter of the points represents the cluster size. Most EV clusters accumulate in the lower left corner. (**E-H**) Examples of non-coding RNAs that increase or decrease with age. The x-axis represents the age, the y-axis the expression of the selected non-coding RNA (orange, EV; blue serum). (**I**) Confusion matrix scatter plots (see also panel (A) split by the RNA classes.

6

202   whether the miRNAs increasing or decreasing with age in vesicles or plasma exhibit a distinct

203   function in a pathway-specific manner. For each gene ontology category[22] we computed an

204   enrichment score for the miRNAs in EVs and in serum. Next, we used the list of miRNAs sorted

205   by their correlation with age to perform cutoff-free miRNA set enrichment analysis[23,24]. A direct

206   comparison provided strong evidence supporting the notion that miRNAs correlated with age

207   in vesicles are significantly enriched in biochemical categories as compared to those in plasma

208   *(Fig. 3A)*. This finding is in line with our initial hypothesis that EVs are specifically loaded with

209   non-coding RNAs that exert biological processes in remote sensing cells. To understand the

210   nature of these processes, we compared the 16 categories that are at least three orders of

211   magnitude more significant in vesicles as compared to plasma to the two being at least three

212   orders of magnitude more significant in serum. In the former, the strongest enrichment was

213   found for the protein heterodimerization activity, neural crest cell migration, negative regulation

214   of inflammatory response, receptor internalization, positive regulation of neuroblast

215   proliferation, the mitochondrial envelope, the positive regulation of DNA-templated

216   transcription and the TORC2 complex (all with adjusted p-value $< 5 \times 10^{-5}$ in vesicles and p-

217   value > 0.01 in serum). The categories with higher significance in plasma are cellular response

218   to BMP stimulus ($p = 6 \times 10^{-5}$ vs. 0.11) and negative regulation of myotube differentiation

219   ($p = 6 \times 10^{-7}$). Distinct pathways being specifically enriched in vesicles opens the question on

220   potential effects in gene regulation in different tissues.

221   The core hypothesis of our work stipulates specific loading of EVs with non-coding

222   RNAs, first and foremost miRNAs, enabling the performance of specific function and gene

223   regulation in remote cells. Previously, we established a bulk- and single cell murine tissue

224   aging atlas, Tabula Muris Senis[7,8]. In these studies, we report both linear and nonlinear aging

225   trajectories in gene expression signals. Similar to the findings on non-coding RNAs observed

226   here, the associated genes cluster with coherent biological functions (among others,

227   extracellular matrix regulation, unfolded protein binding, mitochondrial function, and

228   inflammatory and immune response). The expression patterns are consistent across tissues,

229   differing only in the amplitude and age of onset. Especially fat tissues showed early aging

230   signals of biochemical pathways similar to those observed in the miRNA pathway analysis

231   described above. It was previously shown that miRNAs target genes in a pathway specific

232   manner[25-27]. Thus, for miRNAs associated with age we extracted validated target genes from

233   miRTarbase[28] and evaluated the correlation of potential targets with age annotations from

234   Tabula Muris Senis (*Fig. 3B*). In this context, the expected pattern is a negative correlation of

235   target genes where miRNAs increase with age and vice versa, and as such was confirmed for

236   several organs, including mesenteric fat, gonadal fat, the brain's white blood cells and brown

237   fat. Likewise, the tissue independent aging patterns matched our expectations. While fat

238   tissues generally showed the best concordance, other tissues such as the lung or pancreas

did not. The target gene correlation for mesenteric and gonadal fat verified the increased correlation with age for miRNAs decreasing with age and vice versa (**Fig. 3C/3D**). Intriguingly, this effect was more pronounced for gonadal fat, however only for EV bound miRNAs and less so for serum. Translating the miRNAs and genes to a proper target gene network identified 8 core genes: *Notch1*, *Bace1*, *Hdac4*, *Igf1*, *Eln*, *Cav2*, *Insig1*, and *Scap* (**Fig. 3E**), possibly reflecting physiological relevance for both signaling networks and epigenetic processes.

In sum, our analysis reinforces the central role of fat in early aging processes, indicating that vesicle bound miRNAs have important contributions. Having demonstrated that the cargo of EVs seems to be biologically relevant further opens the question whether it is just the cargo of the EVs or whether the
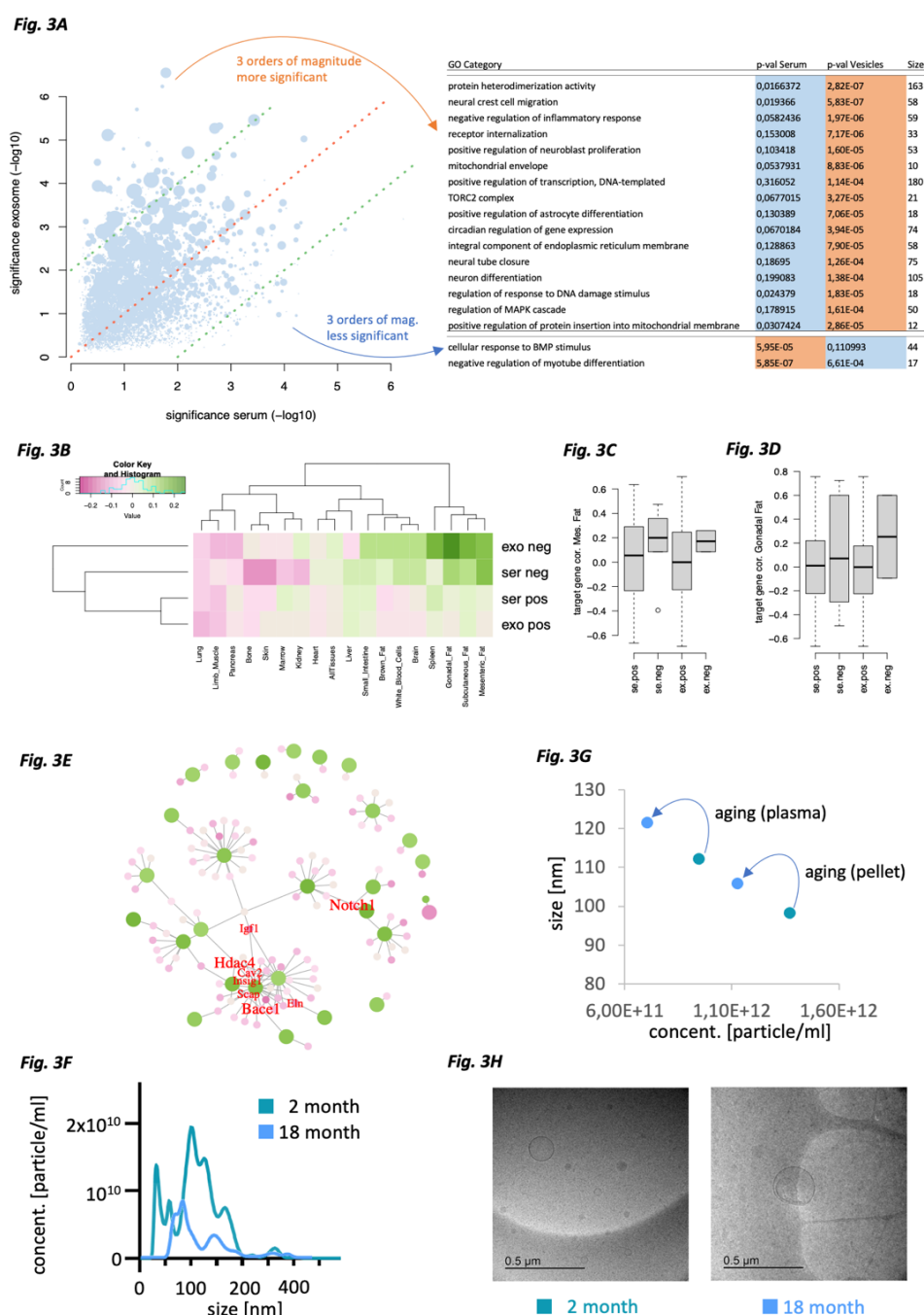

Figure 3: Pathway results and nanoparticle tracking. (**A**) miRNA pathway enrichment for age-related miRNAs in plasma (x-axis) and vesicles (y-axis). Each dot is one pathway, the size represents the number of miRNAs associated with the pathway. The red dashed line is the bisector, the green lines mean two orders of magnitude higher significance in plasma and vesicles, respectively. The pathways with at least three orders of magnitude difference are listed on the right. (**B**) For miRNAs that are positively and negatively correlated with age in plasma and vesicles, the correlation with age of target genes from Tabula Muris Senis across 17 tissues is shown. Expected is that miRNAs going down with age have target genes going up with age and vice versa. (**C,D**) For two fat tissues the target gene correlation with age is detailed for the four groups shown as rows in (B). (**E**) Target network. Large green dots depict genes, small pink dots represent miRNAs and lines delineate regulatory events between miRNAs and genes. The color shading represents the correlation with age and the hub genes targeted by at least three miRNAs are annotated in red. Relative font sizes represent the number of miRNAs targeting the respective gene. (**F**) Size histogram of two selected examples from the nanoparticle tracking analysis, one young and one old mouse. (**G**) Average concentration and size of nanoparticles in young and old mice before and after ultracentrifugation. For both types of analysis we observe the shift towards fewer but larger vesicles in aged mice. (**H**) Selected electron microscopy images of one young and one old mouse plasma sample show EVs and a limited background signal.

275　　　nature of vesicles is altered.

276　　　　　　We finally carried out nanoparticle tracking analysis (NTA) and Cryogenic electron

277　　　microscopy (cryo-EM) on a new cohort of mice. Thereby we focused on the extreme ages, i.e.,

278　　　studied four mice of the youngest and four mice of the oldest age group. A general shift in the

279　　　distribution from more and smaller EVs present in young animals to fewer but larger EVs in old

280　　　animals was observed (*Fig. 3F, Supplemental Fig. 1*). We performed this analysis for

281　　　samples with and without ultracentrifugation to minimize noise in the data. Although this

282　　　analysis is challenging and apoptotic bodies might blur the image, we find for both sample

283　　　types with and without centrifugation identical patterns: aging leads to a decrease of the

284　　　particle concentration and at the same time to an increase of the average particle diameter

285　　　(*Fig. 3G*). Both the differential loading and the different size and number of EVs seem to add

286　　　to the altered molecular aging profiles across tissues. Although only in a qualitative manner,

287　　　also cryo-EM supported the thesis of different sizes and counts for vesicles in young and old

288　　　plasma (examples are presented in *Fig. 3H*, all available cryo-EM images are shown in

289　　　**Supplemental Fig. 2**).

290

291　　　**Discussion**

292　　　　　　While our study presents intriguing new insights into the correlation of EVs and the

293　　　molecular loading of EVs with non-coding RNAs in the context of aging, it is important to

294　　　mention possible limitations and how we took them into account. First, the purification of EVs

295　　　is challenging and bears many pitfalls[20]. Generally, the more purification steps are applied the

296　　　less material is left, requiring a pooling of samples. We decided to have the maximal purity

297　　　possible while still leaving sufficient material for individual sequencing of small RNAs, avoiding

298　　　any pooling. As stated by Schekman et al. [20], healthy skepticism concerning the possible

299　　　connection between exosomal miRNAs and control of gene expression in target cells will

300　　　remain until functional cell culture and animal studies are conducted with exosomes purified

301　　　by rigorous and quantitatively documented procedures. While NTA and cryo-EM do not replace

302　　　such purification, they demonstrate a limited background noise in the used samples. A second

303　　　limitation comes down to the molecular measurement and annotation of the molecules. Having

304　　　reached a high sequencing depth from low input volumes, the data are mapped to the standard

305　　　reference databases. Whether read molecules, e.g., mapping to piRNAs actually represent

306　　　functional piRNAs and not fragments or reads mapping to miRNAs annotated in miRbase are

307　　　representing functional miRNAs, is only partially known, calling for further functional validation

308　　　experiments. These factors have to be addressed in targeted studies with larger cohorts of

309　　　mice and using orthogonal molecular profiling technologies such as RT-qPCR.

Online Methods

Animals: For the non-coding RNA sequencing experiments, we used female C57BL/6N mice at the age in months of 2 (n = 4; body weight (bw): 19-20 g), 6 (n = 4; bw: 25-29 g), 8 (n = 4; bw: 23-26 g), 12 (n = 2; bw: 31 g) and 18 (n = 4; bw: 34-42 g). To assess the spread of vesicles in fat tissues, a second cohort of female C57BL/6N mice was used with an age of 2 (n = 4; bw: 19-20 g) and 18 months (n = 4; bw: 29-41 g). The animals were housed in groups on wood chips as bedding in the conventional animal facility of the Institute for Clinical & Experimental Surgery (Saarland University, Homburg/Saar, Germany). They had free access to tap water and standard pellet food (Altromin, Lage, Germany) and were maintained under a controlled 12-h day/night cycle. This animal study was approved by the local State Office for Health and Consumer Protection and conducted in accordance with the Directive 2010/63/EU and the NIH Guidelines for the Care and Use of Laboratory Animals (NIH Publication #85-23 Rev. 1985).

Blood sampling: The mice were anesthetized by an intraperitoneal injection of ketamine (100 mg/kg bw; Ursotamin®; Serumwerke Bernburg, Bernburg, Germany) and xylazine (12 mg/kg bw; Rompun®; Bayer, Leverkusen, Germany). Subsequently, they were fixed on a heating pad in supine position. After midline laparotomy, a maximal volume of blood (~700-1000 μL) was taken from the vena cava and transferred into plasma tubes (Sarstedt, Nümbrecht, Germany). The blood samples were then centrifuged at 20°C and 10.000 xg for 5 min and the resulting plasma was stored at -80°C until further use.

Purification of EVs: 200 μl of mouse plasma were transferred to 1 mL open-top thickwall polypropylene ultracentrifugation tube (Beckman-Coulter, USA) and diluted with 800 μL of phosphate-buffered saline to prevent the tube from collapsing in the ultracentrifuge vacuum. Samples were centrifuged for 2 h, at 4°C at 100,000 x g using the Type 50.4 Ti fixed-angle rotor (Beckmann-Coulter, USA). Supernatants were carefully removed, and the pellets were resuspended in 20 μL of phosphate-buffered saline. Samples were stored at –80°C until further analyses.

RNA extraction: Total exosomal RNAs were isolated semi-automated using the miRNeasy Micro kit (Qiagen, Hilden, Germany) and Qiacube isolation robot according to the manufacturer's recommendations with addition of 2 μL RNase-free glycogen (20 mg/mL, Invitrogen, Carlsbad, CA, USA) to facilitate RNA precipitation. RNA concentration was measured using Qubit™ microRNA Assay Kit (ThermoFisherScientific, Waltham, MA, USA).

High-throughput RNA-sequencing: Isolated RNA samples were analyzed by Agilent small RNA Chips and 2 ng each (exosomes and supernatants) were used for Illumina compatible library preparation using the D-Plex small RNA Kit (Diagenode, BE). The kits employ 3´-poly A tailing and template switch-based cDNA generation using UMI (unique molecular identifier) tagged template switch oligos. After PCR amplification involving 13 cycles, libraries were purified from TBE-PAGEs. Illumina sequencing was carried out on a HiSeq2500 platform using the High Output mode for 96 cycles.

Nanoparticle-tracking analysis: 1 μl of serum was diluted in 1199 μL, 1 μL of the resuspended pellet was diluted in 999 μL of phosphate-buffered saline, in order to achieve a final concentration between 20 and 120 particles/frame. Samples were then measured on NanoSight (Malvern, UK) at a camera level of 15. For each sample, three captures of 30 s were acquired. Videos were then analyzed at a detection threshold of 5 using NTA 3.4 software.

Cryo-Transmission Electron Microscopy: 3 μL of each sample were transferred to a holey carbon film-coated copper grid (Plano S147-4), blotted for 2 s, and plunged into undercooled

liquid ethane at –165 °C (Gatan Cryoplunge3). The grid was then, under liquid nitrogen, transferred to a cryo-TEM sample holder (Gatan model 914). Low-dose bright-field images were acquired at –170 °C, using a JEOL JEM-2100 LaB6 Transmission Electron Microscope and a Gatan Orius SC1000 CCD camera.

Bioinformatics: The sample primary processing was performed with miRMaster[29] using standard parameters. As output, miRMaster generated a list with the expression of 80,668 RNAs from 10 RNA classes. The data were normalized to expression in one million reads and further processed with R (R 4.0.4 GUI 1.74 Catalina build (7936)). The Venn diagrams were generated using the *eulerr* package from R. Mapping the fraction of variance to different parameters was done using the principal variance component analysis (*pvca*) package. Splines were computed using the *smooth.spline* function with seven degrees of freedom. Color palettes were generated using the *RColorBrewer* package. Smoothed scatter plots were computed using the *smoothScatter* function setting the point number to 500. Clustering was done for highest expressed non-coding RNAs (at least 5 reads per million in at least one sample) using the scaled expression matrix (z-score of each feature). The clustering was performed with the *hclust* function, using the Euclidean distance measure. Clusters were extracted by cutting the dendrograms at 1/1.25 of the maximal height. Heatmaps of target genes were computed using the *heatmap.2* function. The network visualization has been performed using *iGraph*. As input for the network analysis, targets from miRTarbase [28] were used, however, restricted to strong evidence targets. To compute the statistical concordance of RNAs correlated with aging across sample types, a random background distribution with respect to positive and negative correlation was assumed. Briefly, a random distribution would mean that close to 25% of non-coding RNAs is consistently positively regulated in serum and EVs, 25% is consistently negatively correlated with age and 25% in each are positively correlated in the one and negatively correlated in the other specimen type.

Matrix factorization: We predicted the age of samples with respect to three age groups "young" (2 months), "middle" (6-8 months) and "old" (12-18 months). To this end, the expression patterns were split in 20 individual matrices, for each of the 10 non-coding RNA classes and for plasma and EVs. We first normalized the given non-negative Matrix D by dividing all elements by the maximum value in D. To obtain the probabilistic regarding the age groups, we decomposed the matrix D into two further matrices T and P, where P gives us the desired probabilities. T stands for the matrix of the typical age group vectors, i.e., in each entry of a column there is a value representing all entries at this position of all samples belonging to this age group. The matrix P contains the probabilities of each sample to each age group respective to their typical vector in T. We formulated the non-negative matrix factorization as the optimization problem:

Given: $D \in \mathbb{R}^{m \times n}$

Unknown: $T \in \mathbb{R}^{m \times 3}, P \in \mathbb{R}^{3 \times n}$

Solution: $\min_{T,P} \|D - TP\|_F^2$

$$s.t. \quad 0 \le T[i,s] \le 1 \quad \forall i \in \{1,\dots,m\}, \forall s \in \{1,2,3\}$$
$$0 \le P[s,j] \le 1 \quad \forall s \in \{1,2,3\}, \forall j \in \{1,\dots,n\}$$
$$\sum_{s=1}^{k} P[s,j] = 1 \quad \forall j \in \{1,\dots,n\}$$

The first two constraints require all entries of the matrices T and P to lie between 0 and 1. Since we were interested in the percentage of a sample belonging to the three age groups, we also required all columns of the matrix P to sum up to 1 using a numerical solver[30].
We then classified each sample by choosing the index with the highest entry of each column in P and assigned the index as a label to each one. However, the rows of P were invariant to permutations. Here, this means that it is not clear which label corresponds to which age group. Furthermore, a measure of quality for the results was needed. Using the known age, we could construct a ground truth for each sample and calculated the classification accuracy for every permutation. The ground truth used was "young" corresponding to two-month-old mice,

"middle" to six- and eight-months-old and "old" to twelve- and 18-month-old. Finally, we chose the permutation labels which maximize the accuracy and obtain a measure of quality.

Data availability
All sequencing data are freely available from the Sequence Read Archive SRA [reviewer link to the data is available upon request].

Code Availability
The primary data analysis has been performed using miRMaster. miRMaster is available as web service. The source code of miRMaster is not publicly available because of licensing issues. The other analyses have been carried out using standard R packages that are freely available (see Methods Section).

Competing interests
None declared.

Author contributions
FK contributed to data analysis, data interpretation, and writing the manuscript. TK performed the vesicle extraction experiments. NL contributed to the study set up and the interpretation of the analysis. MS contributed to the sequencing of the samples and to the study set up. LG contributed to the versicle purification experiments. NF contributed to the sequencing experiments. AS contributed to the sequencing experiments. TF contributed to the analysis of primary sequencing data. OH contributed to the analysis of the tissue experiments from TMS. AE performed the matrix factorization analysis. MK performed the Cryo EM analysis. JK contributed to the matrix factorization analysis and the interpretation of the results. KW and HM contributed to the tRNA fragments analysis and interpretation. GF contributed to the vesicle extraction and to the study set up. TWC contributed to the analysis and interpretation of the data in the context of the tissue experiments from TMS. EM contributed to the study set up and the interpretation of the results. MWL performed the mouse experiments. AK contributed to study set up, data interpretation and manuscript writing.

Acknowledgements
We appreciate the support of the mouse facility at Saarland university. We appreciate input from the members of the Keller lab.

Funding
This study has partially been funded by the Regional Government of the Saarland and by Saarland University.

Supplementary Materials are available online.

References

1   Wyss-Coray, T. Ageing, neurodegeneration and brain rejuvenation. *Nature* **539**, 180-186, doi:10.1038/nature20411 (2016).
2   Deelen, J. *et al.* A meta-analysis of genome-wide association studies identifies multiple longevity genes. *Nat Commun* **10**, 3669, doi:10.1038/s41467-019-11558-2 (2019).
3   Lehallier, B. *et al.* Undulating changes in human plasma proteome profiles across the lifespan. *Nat Med* **25**, 1843-1850, doi:10.1038/s41591-019-0673-2 (2019).
4   Fehlmann, T. *et al.* Common diseases alter the physiological age-related blood microRNA profile. *Nat Commun* **11**, 5958, doi:10.1038/s41467-020-19665-1 (2020).
5   Horvath, S. & Raj, K. DNA methylation-based biomarkers and the epigenetic clock theory of ageing. *Nat Rev Genet* **19**, 371-384, doi:10.1038/s41576-018-0004-3 (2018).

6   Aramillo Irizar, P. *et al.* Transcriptomic alterations during ageing reflect the shift from cancer to degenerative diseases in the elderly. *Nat Commun* **9**, 327, doi:10.1038/s41467-017-02395-2 (2018).

7   Schaum, N. *et al.* Ageing hallmarks exhibit organ-specific temporal signatures. *Nature* **583**, 596-602, doi:10.1038/s41586-020-2499-y (2020).

8   Tabula Muris, C. A single-cell transcriptomic atlas characterizes ageing tissues in the mouse. *Nature* **583**, 590-595, doi:10.1038/s41586-020-2496-1 (2020).

9   Pastuzyn, E. D. *et al.* The Neuronal Gene Arc Encodes a Repurposed Retrotransposon Gag Protein that Mediates Intercellular RNA Transfer. *Cell* **172**, 275-288 e218, doi:10.1016/j.cell.2017.12.024 (2018).

10   Tkach, M. & Thery, C. Communication by Extracellular Vesicles: Where We Are and Where We Need to Go. *Cell* **164**, 1226-1232, doi:10.1016/j.cell.2016.01.043 (2016).

11   Kern, F. *et al.* Deep sequencing of sncRNAs reveals hallmarks and regulatory modules of the transcriptome during Parkinson's disease progression. *Nature Aging* **1**, 309-322, doi:10.1038/s43587-021-00042-6 (2021).

12   Zhang, Y. *et al.* Hypothalamic stem cells control ageing speed partly through exosomal miRNAs. *Nature* **548**, 52-57, doi:10.1038/nature23282 (2017).

13   Liu, J. *et al.* Exosomal transfer of osteoclast-derived miRNAs to chondrocytes contributes to osteoarthritis progression. *Nature Aging* **1**, 368-384, doi:10.1038/s43587-021-00050-6 (2021).

14   Meulenbelt, I., Ramos, Y. F. M., Baglio, S. R. & Pegtel, D. M. Censoring exosomal crosstalk in osteoarthritis. *Nature Aging* **1**, 332-334, doi:10.1038/s43587-021-00052-4 (2021).

15   DeCastro, J. *et al.* The Microfluidic Toolbox for Analyzing Exosome Biomarkers of Aging. *Molecules* **26**, doi:10.3390/molecules26030535 (2021).

16   D'Anca, M. *et al.* Exosome Determinants of Physiological Aging and Age-Related Neurodegenerative Diseases. *Front Aging Neurosci* **11**, 232, doi:10.3389/fnagi.2019.00232 (2019).

17   Prattichizzo, F. *et al.* Exosome-based immunomodulation during aging: A nano-perspective on inflamm-aging. *Mech Ageing Dev* **168**, 44-53, doi:10.1016/j.mad.2017.02.008 (2017).

18   Machida, T. *et al.* MicroRNAs in Salivary Exosome as Potential Biomarkers of Aging. *Int J Mol Sci* **16**, 21294-21309, doi:10.3390/ijms160921294 (2015).

19   Lee, E. K. *et al.* The involvement of serum exosomal miR-500-3p and miR-770-3p in aging: modulation by calorie restriction. *Oncotarget* **9**, 5578-5587, doi:10.18632/oncotarget.23651 (2018).

20   Shurtleff, M. J., Temoche-Diaz, M. M. & Schekman, R. Extracellular Vesicles and Cancer: Caveat Lector. *Annual Review of Cancer Biology* **2**, 395-411, doi:10.1146/annurev-cancerbio-030617-050519 (2018).

21   Bartel, D. P. Metazoan MicroRNAs. *Cell* **173**, 20-51, doi:10.1016/j.cell.2018.03.006 (2018).

22   Gene Ontology, C. The Gene Ontology resource: enriching a GOld mine. *Nucleic Acids Res* **49**, D325-D334, doi:10.1093/nar/gkaa1113 (2021).

23   Kern, F. *et al.* miEAA 2.0: integrating multi-species microRNA enrichment analysis and workflow management systems. *Nucleic Acids Res* **48**, W521-w528, doi:10.1093/nar/gkaa309 (2020).

24   Backes, C., Khaleeq, Q. T., Meese, E. & Keller, A. miEAA: microRNA enrichment analysis and annotation. *Nucleic Acids Res* **44**, W110-116, doi:10.1093/nar/gkw345 (2016).

25   Kern, F. *et al.* Validation of human microRNA target pathways enables evaluation of target prediction tools. *Nucleic Acids Res* **49**, 127-144, doi:10.1093/nar/gkaa1161 (2021).

26   Kehl, T. *et al.* miRPathDB 2.0: a novel release of the miRNA Pathway Dictionary Database. *Nucleic Acids Res* **48**, D142-D147, doi:10.1093/nar/gkz1022 (2020).

27   Backes, C. *et al.* miRPathDB: a new dictionary on microRNAs and target pathways. *Nucleic Acids Res* **45**, D90-D96, doi:10.1093/nar/gkw926 (2017).

28   Huang, H. Y. *et al.* miRTarBase 2020: updates to the experimentally validated microRNA-target interaction database. *Nucleic Acids Res* **48**, D148-D154, doi:10.1093/nar/gkz896 (2020).

29   Fehlmann, T. *et al.* Web-based NGS data analysis using miRMaster: a large-scale meta-analysis of human miRNAs. *Nucleic Acids Res* **45**, 8731-8744, doi:10.1093/nar/gkx595 (2017).

30   Lutsik, P. *et al.* MeDeCom: discovery and quantification of latent components of heterogeneous methylomes. *Genome Biol* **18**, 55, doi:10.1186/s13059-017-1182-6 (2017).